

# Coherent acoustic vibration of metal nanoshells

C. Guillon<sup>a</sup>, P. Langot<sup>a</sup>, N. Del Fatti<sup>a,b</sup>, and F. Vallée<sup>a,b</sup>

<sup>a</sup> *Centre de Physique Moléculaire Optique et Hertzienne*

*CNRS and Université Bordeaux I, 351 cours de la Libération, 33405 Talence, France and*

<sup>b</sup> *Laboratoire de Spectrométrie Ionique et Moléculaire*

*CNRS and Université Lyon I, 43 Bd. du 11 Novembre 1918, 69622 Villeurbanne, France*

A. S. Kirakosyan and T. V. Shahbazyan

*Department of Physics and Computational Center for Molecular Structure and Interactions,  
Jackson State University, P.O. Box 17660, Jackson, Mississippi 39217, USA*

T. Cardinal and M. Treguer

*Institut de Chimie de la Matière Condensée de Bordeaux*

*CNRS and Université Bordeaux I, 87 Av. du Dr. Albert Schweitzer, 33608 Pessac, France*

(Dated: November 6, 2018)

Using time-resolved pump-probe spectroscopy we have performed the first investigation of the vibrational modes of gold nanoshells. The fundamental isotropic mode launched by a femtosecond pump pulse manifests itself in a pronounced time-domain modulation of the differential transmission probed at the frequency of nanoshell surface plasmon resonance. The modulation amplitude is significantly stronger and the period is longer than in a gold nanoparticle of the same overall size, in agreement with theoretical calculations. This distinct acoustical signature of nanoshells provides a new and efficient method for identifying these versatile nanostructures and for studying their mechanical and structural properties.

Metal nanoshells – metal shells grown on dielectric spheres – are among the highlights of nanostructures with versatile optical and mechanical properties [1]. As for fully metallic nanoparticles, absorption and scattering of light by nanoshells are dominated by the surface plasmon resonance (SPR) [2]. However, they offer wide new possibilities of controlling the SPR characteristics, such as its frequency position, by varying, for instance, the shell thickness vs. overall size, or the constituent materials [3, 4]. Furthermore, recent measurements of scattering spectra of single nanoshells [5, 6] indicated enhanced sensitivity to their environment and narrowing of their resonance lineshape as compared to solid gold particles [7]. These unique tunability and characteristics of nanoshells optical properties spurred a number of proposals for their applications including in optomechanics [8], sensing [9, 10], and drug delivery [11, 12].

While the optical response of nanoshells has been extensively studied, much less is known about their acoustical properties. In fact, the low frequency vibrational modes of nanostructures bear a unique signature of their structural and mechanical properties directly reflecting the impact of confinement on the ionic movement. This is in contrast to the optical frequency domain whose features are determined by the electronic response. The vibrational modes thus constitute additional source of information that could be particularly important in the case of complex systems. This is especially the case for hybrid or layered systems with structurally distinct constituents, such as nanoshells [13, 14]. Due to their structural sensitivity, vibrational modes are also expected to constitute acoustic signatures permitting further nanoshell identification, complementary to the optical one.

Time-resolved optical techniques are powerful tools for investigating the low-frequency vibrational modes of nanostructures. They have been applied to the study of the acoustic properties of semiconductor and metal nanoparticles [15, 16, 17, 18] and have recently been extended to bimetallic particles [19, 20]. In these experiments, vibrational modes are impulsively excited as a result of rapid expansion of metal particle induced by absorption of a femtosecond pump pulse [15, 21]. In this process, the energy initially injected into the electron gas is quickly damped to the lattice on the time scale of the electron-phonon energy transfer, about 1-2 picosecond in noble metals. Due to lattice anharmonicity, this lattice heating leads to an isotropic force on ions triggering in-phase dilation of each particle that subsequently undergoes radial contractions and expansions around its new equilibrium size. The periodic change in nanoparticle volume translates into a modulation in time of the electronic properties. This can be detected by a time-delayed probe pulse monitoring the concomitant modulation of the wavelength of the SPR [15]. The triggered initial expansion being homogeneous, the modulation is dominated by the fundamental breathing mode that closely corresponds to particle expansion as a whole.

Using time-domain spectroscopy, we have performed the first investigation of acoustic vibrational modes in metal nanoshells. As in fully metallic particles, we observed in nanoshells a pronounced time-modulation of the measured probe differential transmission indicating coherent excitation of the fundamental breathing mode. The modulation amplitude is significantly stronger and its period is considerably longer than those in pure gold nanospheres of the same size. At the same time, the

damping time of the oscillations is much shorter than for gold particles suggesting a faster energy transfer from nanoshells to the surrounding medium. Such distinct signatures allow unambiguous identification of nanoshell acoustic vibration and separation of their contribution from that of possibly present other entities in a colloidal solution. These results are consistent with theoretical analysis of vibrational modes in nanoshells.

Experiments were performed in colloidal solution of  $\text{Au}_2\text{S}$ -core/Au-shell nanoshells prepared using the method described in Ref. [1]. Both nanoshells and gold nanoparticles are simultaneously synthesized, as shown by the linear absorption spectra of the colloidal solution (Fig. 1). It exhibits two characteristic bands centered around 700 and 530 nm that have been associated to SPR in core-shell nanoparticles and gold nanospheres, respectively [1, 22]. This assignment is confirmed by the spectral displacement of the former band during nanoshell growth, while, in contrast, the spectral position of the latter remains almost unchanged as expected for small nanospheres [1]. This is further corroborated by TEM measurements showing the presence of large nanoparticles (mean radius  $R_2$  in the 14 nm range) that have been identified as nanoshells, and of smaller ones (mean size of about 4 nm) identified as pure gold [1, 14]. The nanoshell SPR energy is determined by the ratio of the inner to outer radius  $R_1/R_2$ ; the latter was thus estimated by fitting the experimental spectrum with  $A(\omega) = P_p A_p(\omega) + P_s A_s(\omega)$ , where  $P_p$  and  $P_s$  are the volume fractions of nanoparticles and nanoshells, respectively, and  $A_{p,s}(\omega)$  are the corresponding absorbances [1]. For the investigated nanoshells,  $R_1$  ranges from 9 to 10.3 nm with a shell thickness  $d = R_2 - R_1$  of 2.5 to 3.7 nm, i.e.,  $R_1/R_2$  ranges from 0.78 to 0.73 nm.

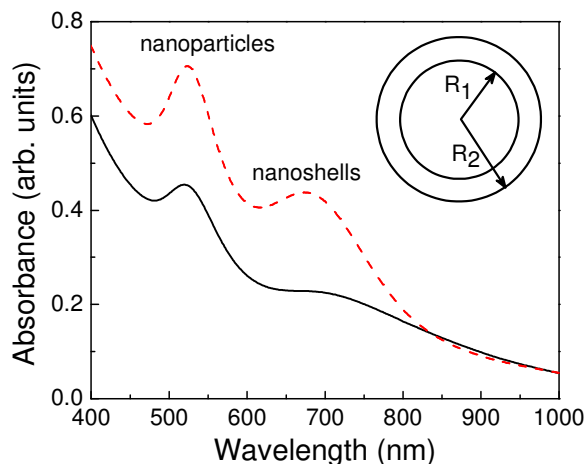


FIG. 1: Measured linear absorption spectrum of  $\text{Au}_2\text{S}$ /Au core/shell particles in water for two different sizes, with  $R_1 = 9.0$  nm inner radius and  $R_2 = 11.5$  nm outer radius (solid line), and for  $R_1 = 11.5$  nm and  $R_2 = 13.5$  nm (dashed line). Inset: schematic geometry of a nanoshell.

Time resolved measurements were performed using a femtosecond Ti:sapphire oscillator delivering 20 fs pulses

at 860 nm with a 80 MHz repetition rate. Part of the pulse train is selected to create the pump pulses. Absorption in this spectral range being dominated by the broad SPR of the nanoshells, they are predominantly excited. The pump induced transient change of the sample transmission  $\Delta T$  is detected at the same wavelength around the nanoshell SPR using the remaining part of the beam. This probe wavelength permits further selection of the nanoshells that thus dominate the detected  $\Delta T/T$  signal. This has been confirmed by the fact that pure gold nanoparticle colloidal solutions yield an undetectable signal in this pump-probe configuration. The two beams were focussed on a 30  $\mu\text{m}$  diameter focal spot and the pump beam average power was about 100 mW. Measurements were performed with a standard pump-probe setup with mechanical chopping of the pump-beam and locking detection of  $\Delta T$ .

The measured time-dependent transmission change shows a fast transient, ascribed to photoexcitation of nonequilibrium electrons and their cooling via electron-lattice energy transfer (Fig. 2). The observed kinetics is consistent with that previously reported in gold nanoparticles and films for similar excitation conditions [23]. This signal is followed by pronounced oscillations that can be reproduced by a phenomenological response function:

$$R(t) = A \exp(-t/\tau) \cos[2\pi t/T_{osc} - \varphi]. \quad (1)$$

using a period  $T_{osc} \approx 38$  ps and a decay time  $\tau \approx 60$  ps for the nanoshells of Fig. 2(a). Such long probe-delay response is similar to that reported in fully metallic nanoparticles [15, 16, 17, 18], but the measured period of the oscillations is by far too long to ascribe them to the residual fully metallic small nanoparticles. We thus ascribed them to the acoustic vibration of the nanoshells. Furthermore, their amplitude relative to that of the short time delay electronic signal, is much larger than in metal nanospheres (about 75% as compared to 10% [15]). The measured period is also much longer (about 4 times) than that predicted for solid Au nanospheres of the same overall size, about 9 ps for  $R_2 = 13.5$  nm. Furthermore, the phase of the oscillation  $\varphi \approx 1.1$  is significantly larger than predicted for a purely displacive type of excitation in a harmonic oscillator model (about 0.2). As this phase is a signature of the excitation mechanism, this suggest a modified launching process as compared to the breathing mode of nanospheres [21].

Measurements performed in different nanoshells show similar behaviors with an almost linear increase of the oscillation period with the outer nanoshell size  $R_2$  [Fig. 2(b)]. The effective decay time  $\tau$  of the oscillations can also be extracted from the time-domain data. It varies from 30 to 60 ps for the three investigated samples (30, 60 and 42 ps in increasing order of  $R_2$ ), but conversely to the period, no systematic variation with the nanoshell size is experimentally found. This suggests that, as for nanosphere colloidal solutions, inhomogeneous relaxation due to the particle size and structure fluctuations dominates over the homogeneous one due to

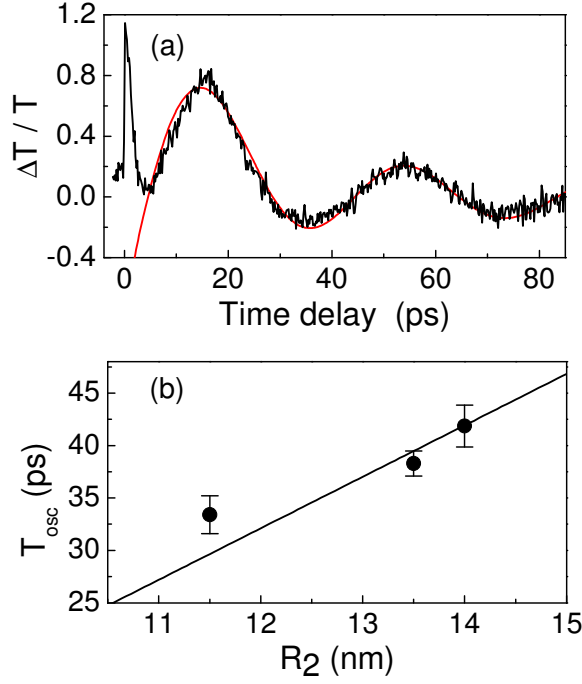


FIG. 2: (a). Time-dependent differential transmission  $\Delta T/T$  measured in  $\text{Au}_2\text{S}/\text{Au}$  nanoshells in water with near infrared pump and probe pulses is shown together with a fit using Eq. (1). The inner and outer radii are  $R_1 = 10.3$  and  $R_2 = 13.5$  nm, respectively. (b) Oscillation period  $T_{osc}$  measured in different  $\text{Au}_2\text{S}/\text{Au}$  nanoshells as a function of their outer radius  $R_2$ . The aspect ratio  $R_1/R_2$  is 0.78, 0.76 and 0.74, in increasing  $R_2$  order. The line is a fit assuming that  $T_{osc}$  is proportional to  $R_2$ .

matrix-water coupling [16, 24].

To further correlate the observed oscillation mode with the nanoparticle structure, we have theoretically analyzed the radial vibrational modes of a spherical nanoshell in a dielectric medium. The motion of nanoshell boundaries is determined by the radial displacement  $u(r)$  that satisfies the Helmholtz equation (at zero angular momentum)

$$u'' + \frac{2u'}{r} + k^2 u = 0, \quad (2)$$

where  $k = \omega/c_L$  is the wave-vector. In the presence of core and outer dielectric medium, the boundary conditions impose that both the displacement  $u(r)$  and the radial diagonal component of the stress tensor,

$$\sigma_{rr} = \rho \left[ c_L^2 u' + (c_L^2 - 2c_T^2) \frac{2u}{r} \right], \quad (3)$$

are continuous at the core/shell and shell/medium interfaces ( $\rho$  and  $c_{L,T}$  are, respectively, density and longitudinal/transverse sound velocities). In the core, shell, and medium regions, solutions are, respectively, of the form  $u \sim [\sin(kr)/r]'$ ,  $u \sim [\sin(kr + \phi)/r]'$ , and  $u \sim [e^{ikr}/r]'$ , where  $\phi$  is the phase mismatch and prime stands for

derivative over  $r$ . Matching  $u$  and  $\sigma_{rr}$  at  $r = R_1, R_2$  yields the equations for the eigenvalues

$$\begin{aligned} \frac{\xi^2 \kappa^2}{\xi \kappa \cot(\xi \kappa + \phi) - 1} - \frac{\eta_c \xi^2 \kappa^2}{(\xi \kappa / \alpha_c) \cot(\xi \kappa / \alpha_c) - 1} + \chi_c &= 0, \\ \frac{\xi^2}{\xi \cot(\xi + \phi) - 1} + \frac{\eta_m \xi^2}{1 + i\xi / \alpha_m} + \chi_m &= 0, \end{aligned} \quad (4)$$

where  $\xi = kR_2 = \omega R_2 / c_L$  and  $\kappa = R_1 / R_2$  are shorthand notations for the normalized eigenenergies and aspect ratio, respectively. The parameters

$$\begin{aligned} \alpha_i &= c_L^{(i)} / c_L^{(s)}, \quad \eta_i = \rho^{(i)} / \rho^{(s)}, \quad \chi_i = 4(\beta_s^2 - \eta_i \delta_i^2), \\ \beta_i &= c_T^{(i)} / c_L^{(i)}, \quad \delta_i = c_T^{(i)} / c_L^{(s)}, \end{aligned} \quad (5)$$

characterize the metal/dielectric interfaces ( $i = c, s, m$  stand for core, shell, and outer medium). From Eq. (4), the ideal case of a nanoshell in vacuum is obtained by setting  $\alpha_c = \alpha_m = \eta_m = \eta_c = 0$  and  $\chi_c = \chi_m = 4\beta_s^2$ ; in the thin shell limit,  $1 - \kappa = d/R_2 \ll 1$ , we then recover the well known result  $\xi_0 = 2\beta_s \sqrt{3 - 4\beta_s^2}$  [26]. For a nanoshell in a dielectric medium, the eigenvalues are complex reflecting energy exchanges with the environment,  $\xi = \omega R_2 / c_L + i\gamma R_2 / c_L$ , where  $\omega = 1/T_{osc}$  and  $\gamma = 1/\tau$  are the mode frequency and damping rate, respectively.

This general model provides an equilibrium description of the nanoshell acoustic response. However, under ultra-fast excitation, the role of the dielectric core is expected to diminish. Indeed, the dielectric core is not directly affected by the pump pulse, but experiences thermal expansion as a result of heat transfer from the metal shell. At the same time, this expansion is much weaker than that of the metal, so that when new equilibrium size is established, the core is almost fully disengaged from the shell. This should be contrasted to bimetallic particles where the core remains engaged after the expansion and thus contributes to the acoustical vibration spectrum [19, 20].

To take into account this effect, calculations were performed for gold nanoshells with disengaged core [ $\eta_c = 0$  in Eq. (4)]. The calculated frequency,  $\omega$ , and damping rate,  $\gamma = 1/\tau$ , are plotted in Fig. 3 versus the aspect ratio  $R_1/R_2$ , for the fundamental breathing mode of nanoshells immersed in water. The data are normalized in units of  $c_L/R_2$  so that the corresponding curves for solid nanoparticles are horizontal lines starting at  $R_1/R_2 = 0$ . The sound velocities and the density were taken as  $c_L^{(s)} = 3240$  m/s,  $c_T^{(s)} = 1200$  m/s,  $\rho^{(s)} = 19700$  kg/m<sup>3</sup> for Au, and  $c_L^{(m)} = 1490$  m/s,  $c_T^{(m)} = 0$ , and  $\rho^{(m)} = 1000$  kg/m<sup>3</sup> for water.

The computed frequency of the fundamental mode is significantly smaller for nanoshells as compared to gold particles of the same overall size (Fig. 3). It is about 2 times smaller for  $R_1/R_2 = 0.5$  and further decreases to about a factor of 3 for thin nanoshells. In contrast, the aspect ratio dependence of the computed damping rate

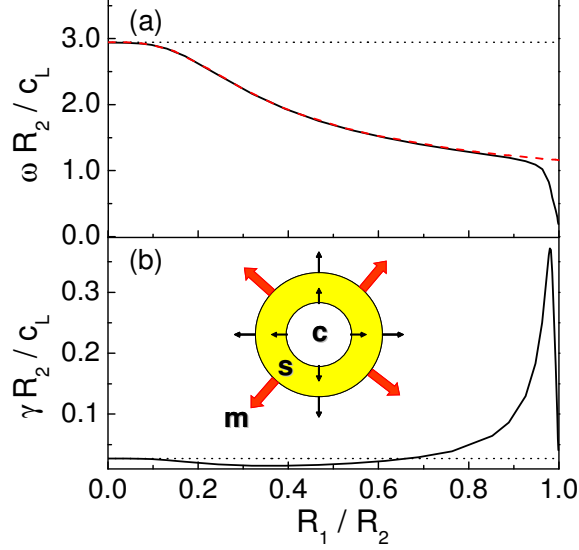


FIG. 3: Calculated frequency (a) and damping rate (b) of the fundamental breathing mode of a gold nanoshell with disengaged core in water versus its aspect ratio  $R_1/R_2$ . The dashed line in (a) is for a gold nanoshell in vacuum. The horizontal dotted lines show the normalized frequency and damping for a gold nanosphere of the same overall size (radius  $R_2$ ). The inset indicates mechanical movement associated to the fundamental mode (thin arrows) and the energy damping mechanism to the environment (thick arrows).

is non-monotonic. A minimum is reached at  $R_1/R_2 = 0.4$ , followed by a large increase for thin shells that can be understood on the basis of energy consideration: the deposited energy is proportional to the nanoshell volume,  $V$ , while the efficiency of energy exchange is determined by the surface area,  $A$ . Then, the characteristic time of energy transfer from the shell to the outer medium is  $\tau \sim V/Ac_L^{(m)} \propto d/c_L^{(m)}$ , as opposed to the  $R/c_L^{(m)}$  dependence for solid particles [25]. With further decrease of the nanoshell thickness, a sharp change in behavior is seen for both  $\omega$  and  $\gamma$ , indicating a crossover to an overdamped regime (Fig. 3). In this thin shell limit, the spectrum of vibrational modes is mostly determined by the energy exchange with environment, as shown by the large deviation of the computed frequency for a water or vacuum environment for  $R_1/R_2 \geq 0.9$  (Fig. 3).

The behavior for the thin shell regime can be better analyzed using approximated analytical solutions for the vibrations frequency and damping. For  $1 - \kappa = d/R_2 \ll 1$ , Eqs. (4) (with  $\eta_c = 0$ ) reduces to

$$\frac{\chi_c}{1 - \kappa} \left( \chi_m - \chi_c + \frac{\alpha_m \eta_m \xi^2}{\alpha_m - i\xi} \right) = \left( \chi_m + \frac{\alpha_m \eta_m \xi^2}{\alpha_m - i\xi} \right) \xi_0^2 - \chi_c \xi^2. \quad (6)$$

In the typical case when the metal shell density is much higher than that of the surrounding medium, i.e.,  $\eta_m =$

$\rho^{(m)}/\rho^{(s)} \ll 1$ , Eq. (6) further simplifies to

$$x^2 - 1 = \frac{\alpha_m \eta_m}{\xi_0 (1 - \kappa)} \left[ \frac{4\alpha_m \beta_m^2}{\xi_0} - \frac{x^2}{\alpha_m / \xi_0 - ix} \right], \quad (7)$$

where  $x = \xi/\xi_0$  and we used  $\chi_m - \chi_c = -4\eta_m \alpha_m^2 \beta_m^2$  and  $\chi_m/\chi_c = 1 - \eta_m \beta_m^2$ . Two regimes can now be clearly identified, governed by the ratio  $\eta_m/(1 - \kappa) = R_2 \rho^{(m)}/d\rho^{(s)} \approx M_m/M_s$ , where  $M_s$  is the metal shell mass, and  $M_m$  is the mass of outer medium displaced by the core-shell particle. Explicit expressions can be obtained for the cases of “heavy” and “light” shells. For a “heavy shell”,  $M_s \gg M_m$ , the complex eigenvalue is given by

$$\xi \simeq \xi_0 - \frac{\lambda}{2} \left[ \frac{\alpha_m + i\xi_0}{(\alpha_m/\xi_0)^2 + 1} - 4\alpha_m \beta_m^2 \right], \quad (8)$$

where  $\xi_0$  is the eigenvalue for a nanoshell in vacuum and  $\lambda = \alpha_m \eta_m / \xi_0 (1 - \kappa)$ . In a good approximation, the real part is simply  $\xi' \simeq \xi_0$ , and is thus independent of the medium or aspect ratio, in agreement with the full calculation for  $R_1/R_2 \leq 0.9$  (Fig. 3). In contrast the imaginary part, although small ( $\xi'' \ll \xi'$ ), is only non-zero in presence of a matrix and thus depends on both. Putting all together, we obtain in the “heavy shell” regime

$$\omega \simeq \frac{2c_L^{(s)} \beta_s}{R_2} \sqrt{3 - 4\beta_s^2}, \quad \gamma \simeq \frac{c_L^{(m)}}{d} \frac{2\eta_m \beta_s^2 (3 - 4\beta_s^2)}{\alpha_m^2 + 4\beta_s^2 (3 - 4\beta_s^2)}. \quad (9)$$

As discussed above, here the damping rate is determined by the shell thickness rather than by the overall size. In the opposite case of a “light shell”,  $M_s \ll M_m$ , the eigenvalue is given by  $\xi \simeq 2\alpha_m \beta_m (\sqrt{1 - \beta_m^2} - i\beta_m)$ , yielding

$$\omega \simeq 2c_T^{(m)}/R_2, \quad \gamma \simeq \omega c_T^{(m)}/c_L^{(m)}. \quad (10)$$

Note that for a light nanoshell in water ( $c_T^{(w)} = 0$ ) the limiting frequency vanishes. In the crossover region, the nanoshell frequency is significantly lower than in vacuum (Fig. 3).

The above theoretical analysis of the nanoshell vibrational modes is consistent with experimental data. In the aspect ratio of interest,  $R_1/R_2 \approx 0.75$ , the fundamental mode period is considerably longer than for a pure metal particle of same overall size. For the investigated particles, the aspect ratio  $R_1/R_2$  lies in the range where the normalized frequency  $\omega R_2/c_L$  varies weakly so the period is almost proportional to  $R_2$ , in agreement with the experimental data [Fig. 2(b)]. A deviation from a simple  $R_2$  dependence towards longer  $T_{osc}$  is apparent for the nanoshell with largest aspect ratio (smallest  $R_2$ ), in agreement with the calculated vibrational modes spectra. However, the measured period for a nanoshell in Fig. 2(a),  $T_{osc} \approx 38$  ps is larger by about a factor of 2 than that calculated for the *ideal* nanoshell. This discrepancy could be attributed to structural inhomogeneity of the metal shell. Its porous (“bumpy”) structure with interstices increases the surface to volume ratio

and, thus, moves the vibrational modes towards that of effectively *thinner* nanoshells. Importantly, such structural defects drive nanoshell acoustical response *away* from solid nanoparticle, as long as the shell is continuous. Note that clusterization or aggregation processes that effectively break the shell geometry will result in an increase, as compared to ideal shell, of the vibration frequency contrary to the experimentally observed reduction. This specific acoustic response can thus be used to unambiguously distinguish different nanoobjects produced during nanoparticle synthesis, such as nanoparticle clusters and nanoshells.

The computed damping rate  $\tau$  is smaller than the experimental one by almost a factor of 1.5. A similar discrepancy has been reported for nanosphere colloidal solutions [15]. In theoretical models, computation is made for one nanoparticle with a given mean geometry. Damping is then associated to energy transfer to the surrounding medium and is thus weak in the case of a water matrix. As a large number of nanoparticles is simultaneously investigated inhomogeneous damping due to dephasing of the coherently excited acoustic oscillations of the nanoparticles is thus expected to play a dominant

role [16, 24]. This statistical effect that reflects the particle size, shape and structure distribution is also probably at the origin of the sample to sample fluctuations of the measured damping rate.

In summary, using a time-resolved pump-probe technique, we have investigated the acoustic vibration of gold nanoshells in colloidal solution. The results clearly show oscillations with a period in the 40 ps range, much longer than expected for pure gold nanospheres. In agreement with our theoretical model, they have been ascribed to fundamental breathing vibration of the gold nanoshells, whose acoustic signature is thus observed here for the first time. Note that such low frequency vibrational modes (in the  $1\text{ cm}^{-1}$  range) are extremely difficult to observe using spontaneous Raman spectroscopy. These results stress the importance of time-resolved studies of acoustic vibrational modes as a new and powerful tool for unambiguous determination of the structure of synthesized nanoobjects via their specific acoustic properties.

C.G., P.L., N.D.F and F.V. acknowledge financial support by Conseil Régional d'Aquitaine. A.S.K and T.V.S. acknowledge financial support by National Science Foundation and by National Institute of Health.

- 
- [1] R. D. Averitt, D. Sarkar and N. J. Halas, *Phys. Rev. Lett.* **1997**, 78, 4217.
  - [2] U. Kreibig and M. Vollmer, *Optical properties of metal clusters* (Springer, Berlin, 1995).
  - [3] S. L. Westcott, J. B. Jackson, C. Radloff, and N. J. Halas *Phys. Rev. B*, **2002**, 66, 155431.
  - [4] E. Prodan, P. Nordlander, N. J. Halas, *Nano Lett.* **2002**, 3, 1411.
  - [5] G. Raschke, S. Brogl, A. S. Sussha, A. L. Rogach, T. A Klar, J. Feldmann, B. Fieres, N. Petkov, T. Bein, A. Nichtl, and K. Kurzinger, *Nano Lett.* **2004**, 4, 1853.
  - [6] C. L. Nehl, N. K. Grady, G. P. Goodrich, F. Tam, N. J. Halas, and J. H. Hafner, *Nano Lett.* **2004**, 4, 2355.
  - [7] T. Klar, M. Perner, S. Grosse, G. von Plessen, W. Spirkel, and J. Feldmann, *Phys. Rev. Lett.* **1998**, 80, 4249.
  - [8] S. R. Sershen, S. L. Westcott, J. L. West, and N. J. Halas, *Appl. Phys. B* **2001**, 73, 379.
  - [9] Y. Sun, Y. Xia, *Anal. Chem.* **2002**, 74, 5297.
  - [10] J. B. Jackson, S. L. Westcott, L. R. Hirsch, J. L. West, and N. J. Halas, *Appl. Phys. Lett.* **2003**, 82, 257.
  - [11] L. R. Hirsch, J. B. Jackson, A. Lee, N. J. Halas, and J. L. West, *Anal. Chem.* **2003**, 75, 2377.
  - [12] C. Loo, A. Lowery, N. J. Halas, J. West, and R. Drezek, *Nano Lett.* **2002**, 5, 709.
  - [13] J. Z. Zhang, A. M. Schwartzberg, T. Norman, C. D. Grant, J. Liu, F. Bridges, and T. van Buuren, *Nano Lett.* **2005**, 5, 809.
  - [14] G. Raschke, S. Brogl, A. S. Sussha, A. L. Rogach, T. A Klar, J. Feldmann, B. Fieres, N. Petkov, T. Bein, A. Nichtl, and K. Krzinger, *Nano Lett.* **2005**, 5, 811.
  - [15] N. Del Fatti, C. Voisin, F. Chevy, F. Vallée, and C. Flytzanis, *J. Chem. Phys.* **1999**, 110, 11484.
  - [16] J. H. Hodak, A. Henglein, and G. V. Hartland, *J. Chem. Phys.* **1999**, 111, 8613.
  - [17] W. Huang, W. Qian, and M. A. El-Sayed, *Nano Lett.* **2004**, 4, 1741.
  - [18] L. Bonacina, A. Callegari, C. Bonati, F. van Mourik, and M. Chergui, *Nano Lett.* **2006**, 6, 7.
  - [19] J. H. Hodak, A. Henglein, and G. V. Hartland, *J. Phys. Chem. B* **2000**, 104, 5053.
  - [20] J. E. Sader, G. V. Hartland, and P. Mulvaney, *J. Phys. Chem. B* **2002**, 106, 1399.
  - [21] C. Voisin, N. Del Fatti, D. Christofilos and F. Vallée, *Appl. Surf. Science* **2000**, 164, 131.
  - [22] A. L. Aden and M. Kerker, *J. Appl. Phys.* **1951**, 22, 1242.
  - [23] C. Voisin, N. Del Fatti, D. Christofilos, and F. Vallée, *J. Phys. Chem. B* **2001**, 105, 2264.
  - [24] C. Voisin, D. Christofilos, N. Del Fatti, and F. Valle, *Physica B* **2002**, 316, 89.
  - [25] V.A. Dubrovskiy and V.S. Morozhnik, *Izv. Earth Phys.* **1981**, 17, 494.
  - [26] A. E. H. Love, *A Treatise on Mathematical Theory of Elasticity*, (Dover, New York 1944).